

Measurement of $F_2^{c\bar{c}}$ at HERA

K. Lipka^a (on behalf of the H1 and ZEUS collaborations)

^a Deutsches Elektronen Synchrotron
Notkestrasse, 85, D-22607 Hamburg, Germany

Recent results on the extraction of the charm contribution, $F_2^{c\bar{c}}$, to the inclusive proton structure function F_2 in deep inelastic ep scattering at HERA are presented. Different methods of charm tagging and measurements of the charm fragmentation function are shown. The issues related to the extrapolation of the visible cross sections to the full phase space are discussed.

1. Introduction

Results on the charm contribution to the proton structure function, F_2^c , at HERA have been published by the H1 and the ZEUS collaborations [1–3]. The data have shown clear evidence that the dynamics of charm production in ep scattering is dominated by the photon gluon fusion process. In this framework the process $e^+p \rightarrow c\bar{c}$ is sensitive to the gluon density in the proton [4] and allows its universality to be tested. Several charm tagging methods are used at HERA. Charm quarks are either tagged by reconstructing charmed hadrons e.g. $D^{*\pm}$, D^\pm and D^0 mesons, or by making use of the long lifetime and large mass of heavy quarks. $F_2^{c\bar{c}}$ is extracted extrapolating the measured cross sections in the phase space of the analysis to the full phase space using the appropriate theory model. When using the lifetime information, the charm and the beauty contributions to the proton structure are extracted simultaneously. The presented analyses partially cover the data from the HERA-II running period, yielding significant integrated luminosity. Therefore, more precise tests of perturbative QCD (pQCD) become possible.

2. Models of charm production

The description of open heavy flavour production in electron proton collisions is based on perturbative QCD. In leading order (LO), the photon gluon fusion process ($\gamma g \rightarrow Q\bar{Q}$) is the dominant

contribution [1]. This treatment has been extended to next-to-leading order (NLO) for which calculations in several schemes are available [5–9]. All approaches assume the scale introduced by the heavy quark mass to be hard enough to apply pQCD and to guarantee the validity of the factorisation theorem.

In the analyses presented here the “massive approach” is adopted, i.e. a fixed order calculation with massive quarks and assuming three active flavours in the proton. The momentum densities of the three light quarks and the gluon in the proton are evolved by the DGLAP equation [10]. The heavy quarks are assumed to be produced only at the perturbative level [5] via photon gluon fusion. Based on the NLO calculations of order α_s^2 in the coefficient functions [5] programs for different applications were developed in the fixed-flavour-number-scheme (FFNS). The Riemersma program [6] is used for the calculation of inclusive quantities of heavy quark production, like $F_2^c(x, Q^2)$, while the HVQDIS program [7,11] allows the calculation of exclusive quantities by providing the four-momenta of the outgoing partons. Both programs are based on the same calculation and use the same input like PDFs, charm mass and factorisation and renormalisation scales. The MRST2004FF and CTEQ5F3 (ZEUS-S-FF) parton densities, $m_c=1.43$ (1.5) GeV and $\mu_r = \mu_f = \sqrt{Q^2 + 4m_c^2}$ are used in the H1 (ZEUS) analyses presented here. The data presented here are also compared to the RAPGAP [12] and CAS-

CADE [13] Monte-Carlo simulations. Both are based on leading order matrix element calculations with the higher order corrections implemented via parton showers. Parton evolution according to the DGLAP equations is used in the RAPGAP simulation. CASCADE implies intrinsic k_t factorisation and parton evolution according to the CCFM [14] equations.

3. Extraction of $F_2^{c\bar{c}}$ using the reconstruction of charmed hadrons

The contribution of charm to the proton structure function can be determined using the measured cross section of charm-tagged events. In the following measurements based on the reconstruction of charmed mesons are presented. The experimental value of $F_2^{c\bar{c}}$ is determined by:

$$F_{2,exp}^{c\bar{c}} = \frac{\sigma_{vis}^{exp}}{\sigma_{vis}^{th}} \cdot F_{2,th}^{c\bar{c}}. \quad (1)$$

Here σ_{vis}^{exp} (σ_{vis}^{th}) denotes the measured (predicted) meson cross section in the visible phase space of the analysis and $F_{2,th}^{c\bar{c}}$ corresponds to the model prediction for $F_2^{c\bar{c}}$ in the full phase space. The visible phase space accessible by the detectors H1 and ZEUS via reconstruction of charmed mesons covers only about 30% of the full phase space. Therefore the determination of $F_2^{c\bar{c}}$ strongly depends on the model used for the extrapolation. In the following, HVQDIS and CASCADE are used as extrapolation models. The extrapolation uncertainties within a single model are estimated by the variation of the input parameters like parton densities, charm quark mass and the renormalisation/factorisation scales as well as by the variation of the charm fragmentation model.

3.1. Cross section measurements

In the following, the charm tagging method via reconstruction of decays of charmed hadrons is illustrated using the $D^{*\pm}$ mesons. The data were collected with the H1 detector, corresponding to an integrated luminosity $L=345 \text{ pb}^{-1}$. D^* are reconstructed in decays $D^* \rightarrow D^0 + \pi_{slow} \rightarrow K + \pi + \pi_{slow}$. The signal is extracted using the mass difference technique from

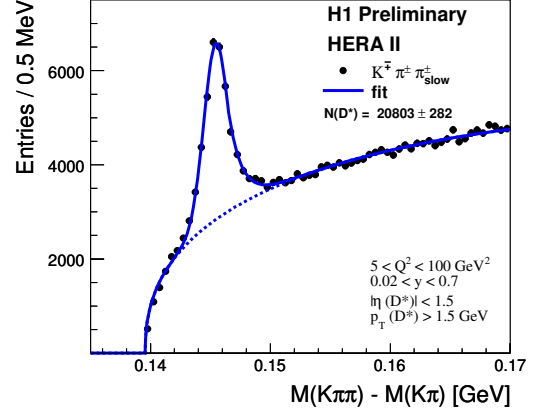


Figure 1. Invariant mass difference of $K\pi\pi$ and $K\pi$ combinations of D^* candidates.

the fit to the Δm distribution of the D^* candidates ($\Delta m = m_{K\pi\pi} - m_{K\pi}$). In Fig. 1 the Δm distribution is shown for the D^* candidates and the wrong charge background. The double-differential cross sections of D^* production as

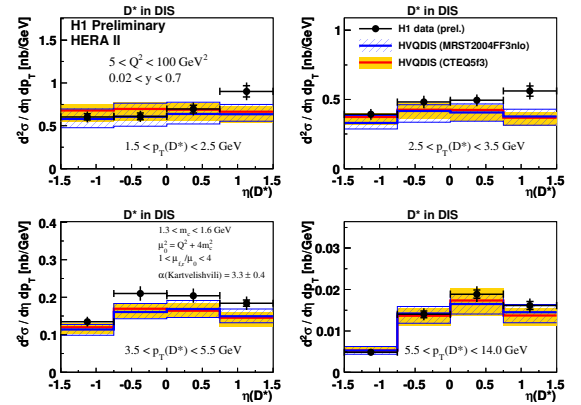


Figure 2. Double-differential D^* cross sections as a function of the pseudo-rapidity η in bins of the transverse momentum p_T . The hatched (shaded) area corresponds to the HVQDIS prediction using the CTEQ5F3 (MRST2004FF3) parton densities. The widths of the bands corresponds to the variation of model parameters.

function of the meson kinematics measured by H1 collaboration are shown in Fig. 2 [15]. The measurements are compared to the NLO calculations using the CTEQ5F3 and MRST2004FF3 parton densities, respectively. Overall the NLO calculation describes the distributions well, however, it seems to underestimate the cross section in the forward region at low $p_T(D^*)$. The dif-

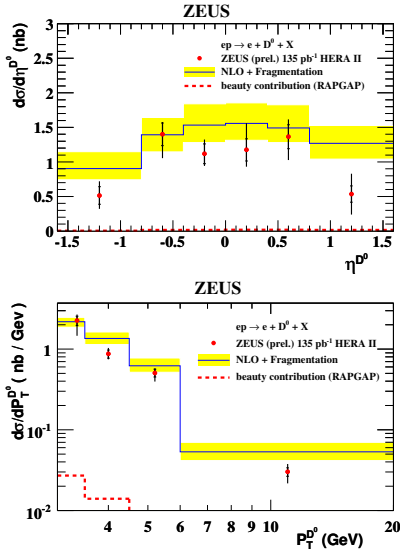


Figure 3. Differential cross section of D^0 -meson production as a function of the meson kinematics, as measured by the ZEUS experiment. The data are compared to the HVQDIS prediction (shaded band) using the ZEUS-S-FF parton densities. The expected beauty contribution is represented by the dotted line.

ferential cross sections of D^\pm and D^0 -mesons are shown in Fig. 3 and Fig. 4 in comparison to the HVQDIS calculation. The data are collected with the ZEUS experiment corresponding to the integrated luminosity of 135 pb^{-1} [16]. The DIS kinematic region $5 < Q^2 < 1000 \text{ GeV}^2$ is explored. The lifetime information from the ZEUS Micro Vertex Detector [17] is used to obtain cleaner D-meson signals in these analyses.

The D^* cross sections are measured [15], [18] in a wide range of Q^2 , as shown in Fig. 5 and Fig. 6. The data are compared to the LO Monte-Carlo

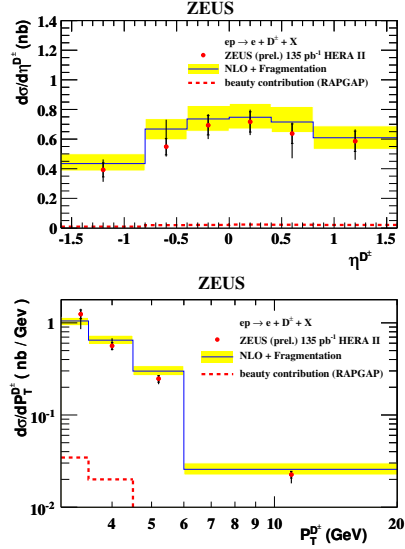


Figure 4. Differential cross section of D^\pm -meson production as a function of the meson kinematics, as measured by the ZEUS experiment. The data are compared to the HVQDIS prediction (shaded band) using the ZEUS-S-FF parton densities. The expected beauty contribution is represented by the dotted line.

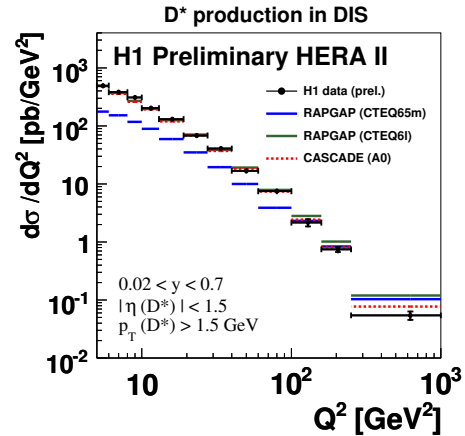


Figure 5. Cross section of D^* meson production as a function of Q^2 as measured by the H1 experiment. The data are compared to the Monte-Carlo simulations RAPGAP using the CTEQ6L (upper solid line) and CTEQ65m (lower solid line) parton densities and CASCADE (dotted line).

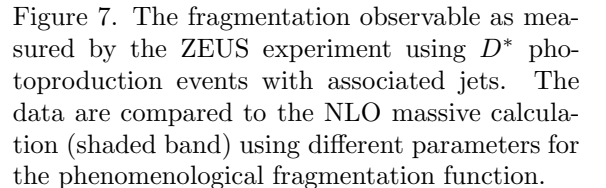


Figure 7. The fragmentation observable as measured by the ZEUS experiment using D^* photoproduction events with associated jets. The data are compared to the NLO massive calculation (shaded band) using different parameters for the phenomenological fragmentation function.

The charm fragmentation function was measured in DIS by the H1 experiment, using data corresponding to an integrated luminosity of 47 pb^{-1} [22]. The energy of the charm quark was approximated by the jet associated to the D^* -meson or by the event hemisphere containing a D^* . The presence of a D^* -associated jet with $E_T > 3 \text{ GeV}$ in the photon-proton rest frame was required, probing the kinematic region significantly above the production threshold. The normalised cross sections are measured as a function of two fragmentation-sensitive observables, z_{jet} and z_{hem} . The data are found to be consistent with the ZEUS measurement and with the prediction of the RAPGAP Monte-Carlo using the fragmentation parameters for heavy quarks ob-

tained from e^+e^- annihilation experiments. This result is consistent with the hypothesis of fragmentation universality between ep and e^+e^- collisions. The hemisphere method is also used to study the charm fragmentation close to the kinematical threshold. This region is defined by the absence of jet with $E_T > 3$ GeV. The result is shown in Fig. 8: the fragmentation parameter extracted for the QCD models in this sample is significantly different from those obtained from the sample above threshold. Thus, the measurements

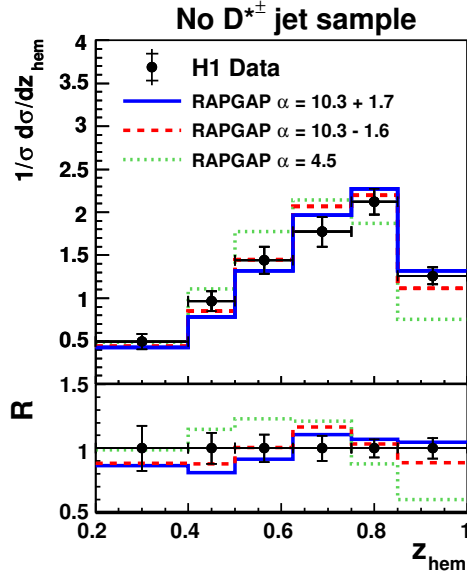


Figure 8. Normalised D^* cross section as a function of z_{hem} for the D^* sample without associated jet. The data are compared to the RAPGAP Monte-Carlo predictions using the Kartvelishvili fragmentation function. The solid and dashed line correspond to $\pm 1\sigma$ variation around the best fit value of α . The dotted line shows the prediction using α fitted to the D^* -jet sample. The ratio $R = \text{model}/\text{data}$ is shown as well as the relative statistical (inner error bar) and systematic uncertainties added in quadrature (outer error bars) for the data points put to $R=1$.

of the charm fragmentation function at HERA indicate a lack of understanding of charm fragmentation close to the production threshold.

3.3. Extraction of $F_2^{c\bar{c}}$

The contribution of charm events $F_2^{c\bar{c}}$ to the proton structure function F_2 is determined according to Eq. 1 in bins of Q^2 and y using a certain extrapolation model. The double-differential cross section of D^* meson production as measured by the H1 experiment is shown in Fig. 9.

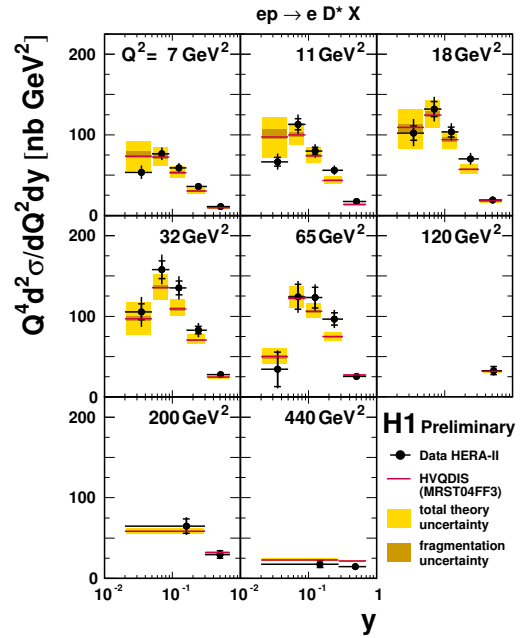


Figure 9. Double differential D^* cross sections compared to the HVQDIS calculation. The solid line corresponds to the central value of the prediction. The charm quark mass has been varied from $m_c = 1.3$ GeV to $m_c = 1.6$ GeV, the renormalisation and factorisation scales have been varied simultaneously $0.5\mu < \mu_r = \mu_f < 2\mu$. The light shaded band represents the full theory uncertainty, obtained from the variations of the charm mass, renormalisation and factorisation scales and the fragmentation model. The dark shaded band shows the theory uncertainty alone from the variations in the fragmentation model.

Predicted visible differential cross sections are calculated using the HVQDIS program after

fragmenting the charm quarks in the photon-proton centre of mass frame into D^* mesons. The Kartvelishvili fragmentation function is used. Following the line of the experimental observation [22], an \hat{s} -dependent charm fragmentation function is used: close to threshold (small \hat{s}) a harder fragmentation parameter is chosen than at large \hat{s} .

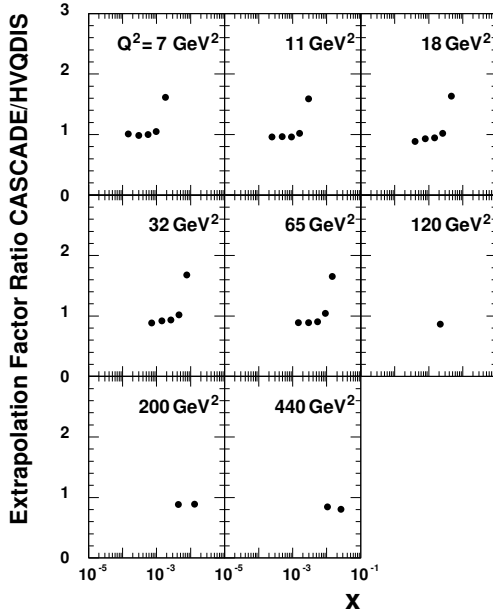


Figure 10. The ratios of extrapolation factors from the visible to the full phase space as obtained by the models CASCADE and HVQDIS.

The extraction of $F_2^{c\bar{c}}$ according to Equation 1 is faced with the problem that the measurement covers only about 20% to 60% of the total phase space for charm production, with the lowest acceptance at large x in the low Q^2 region. Thus the extrapolation depends significantly on the used model. To investigate this model dependence $F_2^{c\bar{c}\text{ exp}}$ is determined using both the NLO DGLAP calculation HVQDIS and the LO Monte-Carlo simulation CASCADE. Both models give a reasonable description of the differential cross sections in both the event kinematics and the kinematics of the D^* meson. The ratios of the extrapolation factors from the visible range to the

full phase space, estimated by using CASCADE and HVQDIS, are shown in Fig. 10. Overall only small differences are observed. However at high x and low Q^2 , the two models differ almost by a factor of 2. The origin of these differences is probably not related to the different parton evolution schemes but rather to the hadronisation models which is currently under investigation.

The measurement of $F_2^{c\bar{c}}$ in the kinematical region $5 < Q^2 < 1000 \text{ GeV}^2$, using the HVQDIS calculation, is shown in Fig. 11

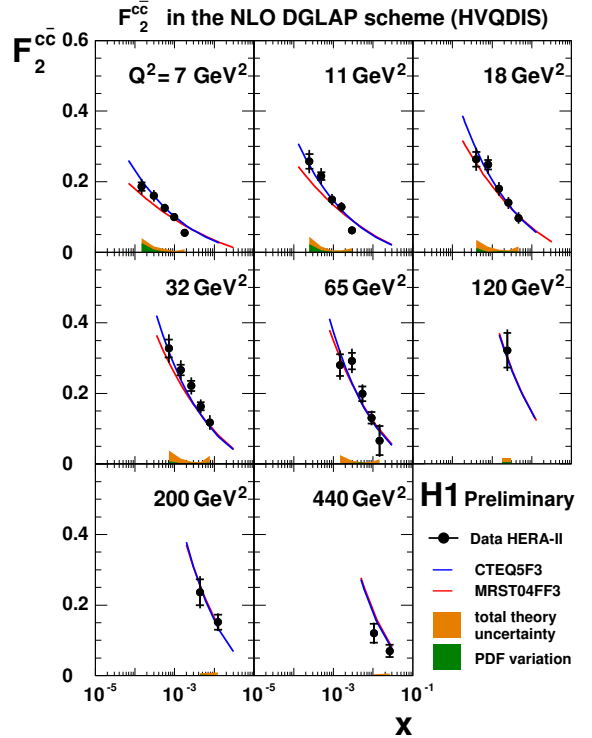


Figure 11. The charm contribution, $F_2^{c\bar{c}}$, to the proton structure function using HVQDIS for the extrapolation. The measurements are compared to the NLO FFNS prediction using the CTEQ5F3 (upper line) and MRST2004FF3 (lower line) parton densities. The extrapolation uncertainty, estimated by variation of the renormalisation and factorisation scales and the fragmentation parameters as well as by a variation of parton densities, is shown by the lighter shaded band. The uncertainty alone due to variation of PDFs is shown by the dark band.

Figure 12. The muon transverse momentum wrt. the associated jet axis as measured in semi-leptonic decays by the ZEUS experiment. The data are compared to the RAPGAP Monte-Carlo (light solid line). The prediction for the charm contribution is shown by the dark solid line. The contribution from b-quarks is indicated by the shaded area. The light flavour (uds) background is depicted by the dashed line.

In Fig. 12 the inclusive distribution of the muon transverse momentum with respect to the associated jet axis, $p_{T,\mu}^{rel}$, is shown. From comparison

of the data to the predicted charm, beauty and uds cross sections the contribution of the specific flavour is determined. The single differential cross sections as functions of the muon kinematics are shown in Fig. 13 and Fig. 14 compared to the HVQDIS calculation.

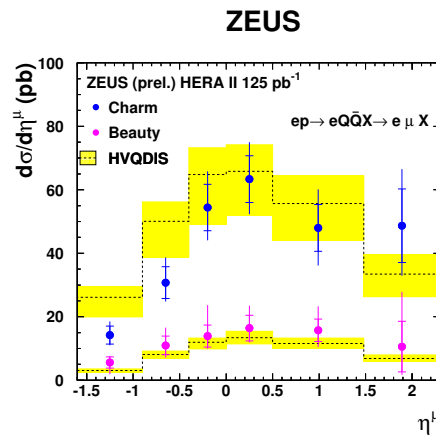


Figure 13. Single differential cross section of muons from b- and c- semi-leptonic decays as function of the muon pseudo-rapidity. The cross sections of beauty (lower data points) and charm (upper data points) are compared to the NLO prediction (shaded band).

The contribution of charm and beauty events to the inclusive proton structure function as determined from the semi-muonic decays is shown in Fig. 15. The HVQDIS calculation was used for the extrapolation. The parton density sets ZEUS-S-FF and CTEQ5F3, the charm mass $m_c = 1.5 \pm 0.2$ GeV and the renormalisation/factorisation scales $\mu_f = \mu_r = \sqrt{Q^2 + 4m_c^2}$ are used. The phenomenological Peterson [24] fragmentation function, defined by a single parameter $\epsilon = 0.055$, was used.

In a similar way, the inclusive charm and beauty reduced cross sections are measured at the H1 experiment in the kinematic region of $5 < Q^2 < 650$ GeV² and $0.0002 < x < 0.032$ [25]. The data correspond to an integrated luminosity of 189 pb⁻¹. The charm and beauty fractions are determined using the observables determined

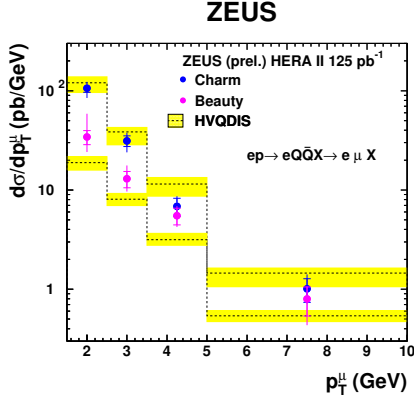


Figure 14. Single differential cross section of b- and c- semi-leptonic decays as function of the muon transverse momentum. The beauty (lower data points) and charm (upper data points) cross sections are compared to the NLO prediction (shaded band).

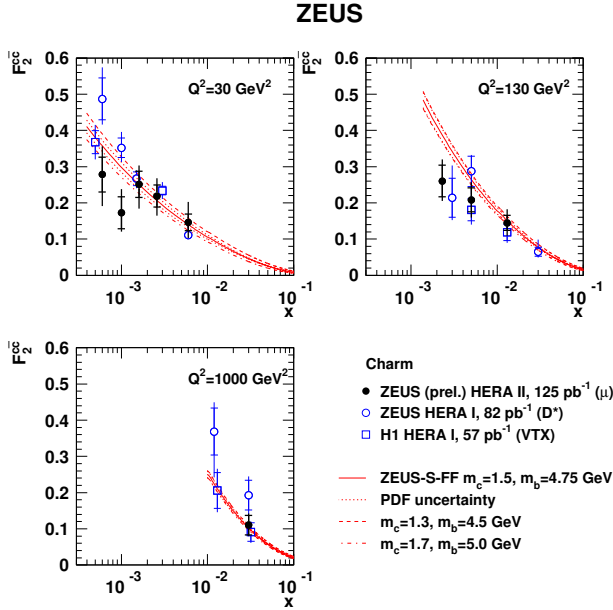


Figure 15. The charm contribution to the proton structure function extracted from the semi-muonic events. The data are compared to the NLO FFNS prediction (solid line) using the ZEUS-S-FF parton density functions. Dash-dotted lines correspond to the variation of c- and b-quark masses.

with help of the H1 central vertex detector. The most important of these observables are the transverse displacement of tracks from the primary vertex and the reconstructed position of the secondary vertex in the transverse plane. The charm and beauty reduced cross sections are presented in Fig. 16.

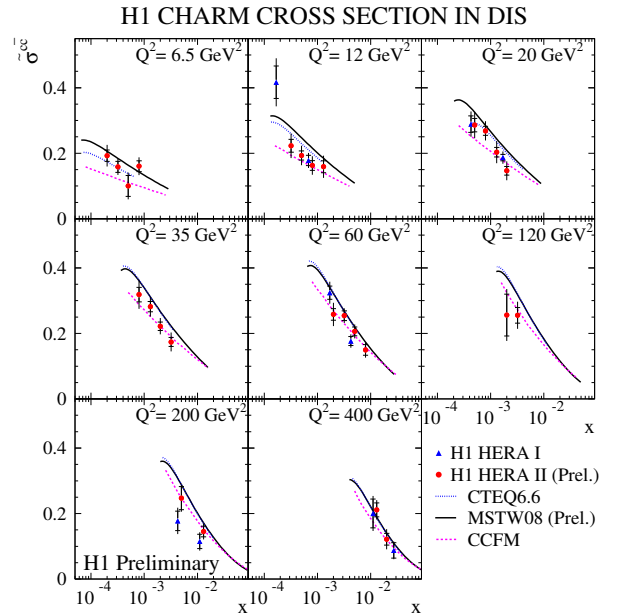


Figure 16. The reduced charm cross section as a function of x in different Q^2 bins. The inner error bars represent the statistical and the outer error bars represent the statistical and systematic uncertainties added in quadrature. The data are compared to different QCD predictions.

The measurements are compared with two recent NLO QCD predictions based on the variable flavour number scheme (VFNS) from CTEQ [26] and MSTW [27] as well as with prediction based on the CCFM parton evolution. The predictions provide a reasonable description of the present data. In Fig. 17 $F_2^{c\bar{c}}$, extracted from the reduced cross section after small corrections for $F_L^{c\bar{c}}$, is compared to the NLO and NNLO models from the MSTW group [28]. While the NLO prediction by the MSTW group seems to overestimate

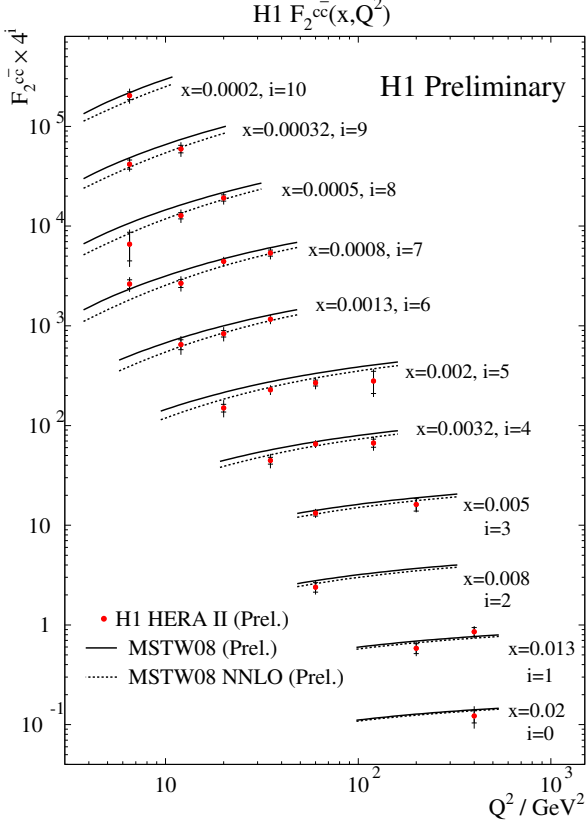


Figure 17. Measured $F_2^{c\bar{c}}$ as a function of Q^2 for different values of x . The data are compared to the MSTW NLO (solid line) and NNLO (dashed line) predictions.

$F_2^{c\bar{c}}$, the NNLO one is in much better agreement with the data.

5. Summary

The recent measurements of the charm contribution $F_2^{c\bar{c}}$ to the inclusive structure function at HERA are approaching the final precision. The distinction power of the measurements with respect to the recent developments of the QCD models in NLO and NNLO has significantly increased. The harvest of the current $F_2^{c\bar{c}}$ measurements at HERA is shown in Fig. 18. Together, the H1 and ZEUS experiments collected data amounting to an integrated luminosity of about 600 pb^{-1} . Both experiments are working on further improvements in both, statistical and sys-

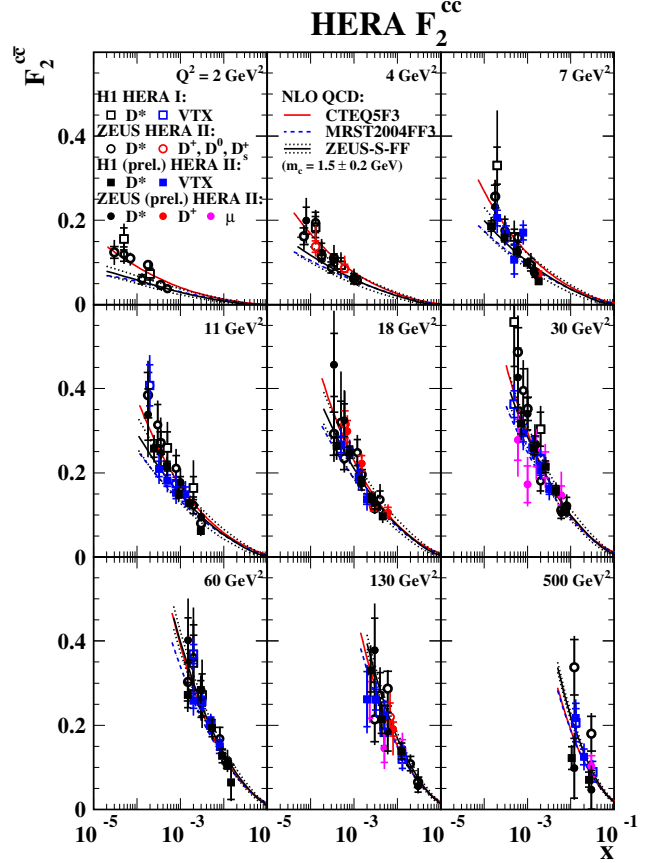


Figure 18. $F_2^{c\bar{c}}$ measurements at HERA as a function of x for different values of Q^2 compared to different QCD predictions.

tematic uncertainties of the measurement. Different charm tagging methods show consistent results and will be combined taking into account proper correlations between the data points and the measurement methods. The results of both collaborations will be combined, thereby the improvement in precision is expected. The extrapolation problems has to be studied further to reduce the theory uncertainty. The charm fragmentation function close to the production threshold has to be studied in more details. Taking into account the contribution of charm events to F_2 in the global PDF fits will put an important constrain on the gluon distribution, which is of the crucial issues for the physics at the LHC.

REFERENCES

1. C. Adloff *et al.* [H1 Collaboration], Z. Phys. C **72** (1996) 593.
2. J. Breitweg *et al.* [ZEUS Collaboration], Phys. Lett. B **407** (1997) 402.
3. J. Breitweg *et al.* [ZEUS Collaboration], Eur. Phys. J. C **12** (2000) 35.
4. C. Adloff *et al.* [H1 Collaboration], Nucl. Phys. B **545** (1999) 21.
5. E. Laenen *et al.*, Phys. Lett. B **291** (1992) 325.
6. E. Laenen *et al.*, Nucl. Phys. B **392** (1993) 162, 229; S. Riemersma, J. Smith, and W.L. van Neerven, Phys. Lett. B **347** (1995) 143.
7. B.W. Harris and J. Smith, Nucl. Phys. B **452** (1995) 109; Phys. Lett. B **353** (1995) 535.
8. M.A.G. Aivazis *et al.*, Phys. Rev. D **50** (1994) 3102.
9. J.C. Collins, Phys. Rev. D **58** (1998) 094002.
10. V. Gribov and L. Lipatov, Sov. J. Phys. **15** (1972) 438 and 675; L. Lipatov, Sov. J. Phys. **20** (1975) 94; G. Altarelli and G. Parisi, Nucl. Phys. B **126** (1977) 298; Y. Dokshitser, Sov. J. Phys. **46** (1977) 641.
11. B.W. Harris and J. Smith, Phys. Rev. D **57** (1998) 2806.
12. H. Jung, Comput. Phys. Commun. **86** (1995) 147.
13. H. Jung, hep-ph/9908497.
14. M. Ciafaloni, Nucl. Phys. B **296** (1988) 49; S. Catani, F. Fiorani and G. Marchesini, Phys. Lett. B **234** (1990) 339; S. Catani, F. Fiorani and G. Marchesini, Nucl. Phys. B **336** (1990) 18; G. Marchesini, Nucl. Phys. B **445** (1995) 49, hep-ph/9412327.
15. [H1 Collab.], contributed papers to the 34th International Conference on High Energy Physics (ICHEP) 2008, abstract Nr. 855 and 860, H1prelim-08-072, H1prelim-08-074.
16. [ZEUS Collab.], contributed paper to European Conference on High Energy Physics (EPS) 2007, abstract Nr. 107.
17. I. Brook *et al.* [ZEUS Collaboration], Nucl. Instrum. Meth. A **581** (2007) 656.
18. [ZEUS Collab.], ZEUS-prel-06-021.
19. [ZEUS Collab.], ZEUS-prel-07-010, hep-ex/0901.1210.
20. S. Frixione, P. Nason and G. Ridolfi, Nucl. Phys. B **454** (1995) 3.
21. V.G. Kartvelishvili, A.K. Likhoded and V.A. Petrov, Phys. Lett. B **78** (1978) 615.
22. F.D. Aaron *et al.* [H1 Collaboration], to be published in Eur. Phys. J. C, hep-ex/0808.1003.
23. [ZEUS Collab.], ZEUS-prel-08-007.
24. C. Peterson *et al.*, Phys. Rev. D **27** (1983) 105.
25. [H1 Collab.], contributed paper to the 34th International Conference on High Energy Physics (ICHEP) 2008, abstract Nr. 834, H1prelim-08-173.
26. P.M. Nadolsky *et al.*, hep-ph/0802.0007.
27. G. Watt, A.D. Martin, W.J. Stirling and R.S. Thorne, hep-ph/0806.4890.
28. R.S. Thorne, Phys. Rev. D **73** (2006) 054019, hep-ph/0601245.